氏　　名(国籍)	NGUYEN (ヌエン) ANH (アン) THI (チ) VAN (ヴァン)
学位の種類	博　　士　(　農　学　)
学位記番号	農　博　第　771　号
学位授与年月日	平　成　16　年　3　月　25　日
学位授与の要件	学位規則第 4 条第 1 項該当
研究科専攻	農学研究科応用生命科学専攻 (博士課程)
学位論文題目	Single-Molecule Imaging of Assembly and Pore-Formation of Staphylococcal γ -Hemolysin on Erythrocyte Membranes (黄色ブドウ球菌γ－ヘモリジンの「一分子技術」による膜孔形成機構の解明)
論文審査委員	(主　査)　教　授　神尾好是 (副　査)　教　授　勝亦瞭一 教　授　西森克彦

論 文 内 容 要 旨

1. INTRODUCTION

Assembly of large macromolecular complexes such as membrane channels and cytoskeletal elements is essential for cell function. A crucial problem of protein complex assembly is to understand mechanism of assembly processes by elucidating information on the beginning, intermediate, and final stages involved (Alberts et al., 2002). Heterogeneous populations of intermediate states, however, are not readily analyzed using ensemble-averaged data. By contrast, single-molecule imaging methods provide direct information about individual intermediate states. At high concentrations of proteins, oligomers could be distinguished from crowded monomers using fluorescence resonance energy transfer between single pairs of acceptor and donor fluorophores (single-FRET) because the acceptor only emits fluorescence if located within several nanometers of the donor.

Pore-forming toxins of bacteria are excellent models for studying the nature of assembly for oligomeric molecules on membranes because of the high stability of recombinant monomeric subunits in solution. *Staphylococcus aureus* Leukocidin fast fraction (LukF) and γ-hemolysin second component (HS) are water-soluble proteins that assemble into hetero-oligomeric pores of γ-hemolysin on membranes of human red blood cells. The pore has a ring-shaped structure with inner and outer diameters of about 2 and 8 nm, respectively.

Using the powerful single-FRET method, we first directly observed the sequential assembly stages of single LukF and HS monomers into oligomers on erythrocyte membranes under the total internal reflection fluorescent TIRF-microscope. As LukF and HS lack cysteine residues, we created single-cysteine LukF and HS mutants which are specifically labeled with donor and acceptor dyes, respectively. We developed a method to calculate the number of subunits in individual oligomers based on the intensity of FRET and direct acceptor signals. We distinguished multiple species of intermediate oligomers, and measured equilibrium association constants of sequential intermediate stages.

The final stage, formation of functional oligomeric pores is also great of interest. This has been extensively studied previously for the related α–hemolysin, based on various biochemical detection methods, but not by direct observation. By contrast with α–hemolysin, intermediate pre-pores have never been obtained so far for the staphylococcal bi-component toxins. The LukF monomer shares a similar basic structure with the α-hemolysin protomer (Fig. 7B), a subunit of the staphylococcal α-hemolysin heptameric pore. The LukF monomer consists of three domains, and three functions have been ascribed to these domains: the rim domain is for membrane binding, the β-sandwich (cap) domain is for oligomerization with Hlg2 and the pre-stem domain is for membrane insertion to lyse the cell. The major differences between LukF and α-hemolysin protomers

are the structures of pre-stem domain. The LukF pre-stem domain folds back against the cap domain, while in α-hemolysin, it makes a long excursion into the lipid bilayers. To elucidate the mechanism of pore-formation for γ-hemolysin and the role of LukF pre-stem domain, we detected the structural changes of the LukF stem domain and observed in real-time Ca^{2+} efflux through the opening pores by a sensitive fluorescent dye (Rhod2). We designed two double-cysteine mutants of LukF whereby the pre-stem domain is trapped by an internal covalent disulfide bond formation, so that several intermediates would be arrested and then released to proceed to pore formation on exposure to a reducing reagent. These two mutants in fact partially assemble into different types of pre-pores that then transit into fully functional pores on the addition of a reductant.

2-3. RESULTS and DISCUSSION

2. Single-molecule imaging of cooperative assembly of LukF and HS into oligomers

2.1. Results

2.1.1. Cooperative binding of HS in the presence of LukF

Single-cysteine mutants of LukF (S45C) and HS (K222C) have single cysteines locating on the top of the respective cap domains (Fig. 1A). Hemolytic activity of the labeled mutants was the same as that of wild-type proteins.

We verified binding constants (K_F, K_H) and the number of binding sites per μm^2 of erythrocyte membranes (R_F, R_H) for individual components. K_F, R_F, K_H and R_H were calculated from the fitted curves shown in Fig. 2A. LukF bound strongly to membranes with a K_F of 2.1×10^{-4} μm^2 and a large number of binding sites (R_F) of 2.0×10^4 μm^{-2}. By contrast, a lower binding constant (K_H, 1.2×10^{-5} μm^2) combined with a similar number of binding sites (R_H, 1.8×10^4 μm^{-2}) indicated a 15-fold decrease in the extent of binding of HS compared with that of LukF. At a given $[F_o]$, $[F_b]$ slightly increased even in the presence of HS at 5-fold higher concentrations than LukF (Fig. 2B1). Meanwhile the binding of HS was obviously enhanced by LukF: $[H_b]$ at a given $[H_o]$ was increased with $[F_o]$. With the same $[F_o]$ and $[H_o]$, HS bound ~ 4 times more than it did without LukF (Fig. 2B2). We demonstrate that both LukF and HS can spontaneously bind to HRBC membranes, but with different binding constants, and that LukF obviously enhances the membrane binding of HS.

2.1.2. Individual monomers and dimers on the membranes

We visualized assembly of LukF-TRM and HS-IC5 on the membranes, at equilibrium, under a TIRF-microscope. At very low concentrations of the two proteins, only a few punctate FRET-IC5 spots, ranging from 0 to 10, were observed on each cell. To calculate the numbers of LukF-TMR (**m**) and HS-IC5 (**n**) in individual FRET-IC5 oligomers ($F_m \cdot H_n$), the occurrence of stepwise decays in the fluorescence intensity was measured. (Fig. 3B4). Those single-FRET spots are dimers containing one LukF and one HS (**F•H**).

The FRET-IC5 intensity ($I_{FRET-IC5}$) were well fitted in a Gaussian distribution with mean of 0.87 ± 0.25 relative to IC5 intensities excited by the red laser.. And FRET efficiency was 87± 10 % relative to the TMR intensity in dimers, indicating a distance between LukF-TMR and HS-IC5 in a dimer of ~ 4.5 nm. The equilibrium association constants for dimerization $K_{F\text{-}H}$ (= $[F\text{•}H] \times [F_1]^{-1} \times [H_1]^{-1}$) were also estimated, based on the concentrations of monomers ($[F_1]$ = 3.8 and $[H_1]$ = 6.9 μm^{-2}) and dimers ($[F\text{•}H]$ = 0.026 μm^{-2}) on the cell membranes (number of cells = 37), to be 0.0010 ± 0.0003 μm^2 (Table 1).

2.1.3. Tetramerization: the dimer-dimer interaction

In assembly of LukF and HS into dimers and other small oligomers, most of the individual FRET intensities were equal to or twice the value of the single-FRET intensities measured in Fig. 3B. **m** and **n** in $F_m\text{•}H_n$ were deduced from the number of steps observed during photobleaching of FRET-IC5 and IC5 signals (Fig. 3C4 and C5).

A tetramer could be formed by two pathways (i) tetramerization of two dimers [F•H + F•H → $(F\text{•}H)_2$] or (ii) "step-by-step" oligomerization of monomers [F•H + F → $F_2\text{•}H_1$ + H→ $(F\text{•}H)_2$ or F•H + H → $F_1\text{•}H_2$ + F → $(F\text{•}H)_2$]. To test which is the main pathway, we measured the association constants for each stage from the concentrations of oligomeric intermediates ($K_{F2\cdot H}$, $K_{F\cdot H2}$ and $K_{(F\cdot H)2}$ in Table 1; appendix 2). Association constants for "dimer-dimer" tetramerization, $K_{(F\cdot H)2}$ = 3.8 μm^2, were > 30 times those for the step-by-step processes, $K_{F2\cdot H}$ = 0.081 μm^2 and $K_{F\cdot H2}$ = 0.12 μm^2. This result could be interpreted as the step-by-step pathway being of far less significance than the dimer-dimer pathway.

2.1.4. Assembly into a single pore: a cooperative step

Various intermediates from dimers to larger oligomers could be obtained at intermediate concentrations (Fig. 4). Individual FRET intensities were ~1, ~2 and ~3 times the single-FRET intensity of F•H (Fig. 4A2 and 4B). The multi-FRET efficiencies of representative spots was also ~90% (Fig. 4C), indicating a close distance between LukF and HS components in larger oligomers.

The histogram of FRET intensities was fitted as the sum of three Gaussian distribution curves (Fig. 4B). The spots at intensity ~3 were more abundant than that at ~2, and ~4. Assuming the area under each Gaussian curve is proportional to the number of oligomers, F•H, $(F\text{•}H)_2$, and $F_3\text{•}H_{3-4}$, we estimated sequential association constants $K_{(F\cdot H)2}$, and $K_{F3\cdot H3-4}$ to be 3.1 and 37 μm^2, respectively (Table 1). As single γ-hemolysin pores have been reported as hexamers and/or heptamers, $K_{F3\cdot H3-4}$ was assigned as the association constant for single a pore, K_p. Obviously, K_p was > 10 times $K_{(F\cdot H)2}$, suggesting that LukF prefers assembling with HS into hexameric and/or heptameric pores $F_3\text{•}H_{3-4}$ rather than into tetramers $(F\text{•}H)_2$.

2.1.5. Assembly into clusters of pores

At higher protein concentrations (15-100% hemolysis), the number of pores incorporated into each FRET spot was deduced from the FRET intensity of the spot divided

by 3 times the single-FRET intensity. The occurrence of single pores and clusters on the membranes was plotted as a histogram in Fig. 5B. Association constants of single pores into two (K_{2p}), three (K_{3p}) and four pores (K_{4p}) were 1.1, 2.7, and 3.4 μm^2, respectively, as shown in Table 1. Those increasing values indicate that single pores tend to assemble into 3-pore or 4-pore clusters rather than into 2-pore clusters.

When LukF-TMR and HS-IC5 were increased over the concentrations that start causing 100% hemolysis (Fig. 5C), the power of the green excitation was reduced to 2.5%. Very highly intense domains of multi-molecular FRET-IC5, probably clusters of pores, could be observed. We plotted a distribution of clusters with various numbers of pores on the membranes in Fig. 6A, blue circles.

2.1.6. Calculating the population of intermediate states

Taking the binding and association constants (Table 1), we estimated the theoretical distribution of intermediates and the total number of pores at given concentrations of proteins. Assuming that K_{np} (n>2) values are similar to K_{3p} and K_{4p} (3 μm^2), at certain $[F_o]$ and $[H_o]$, for example 25 and 1000 μm^{-2}, the distribution of monomers and oligomers could be calculated (Fig. 6A). Populations of clusters of pores (Fig. 6A, blue circles) used in Fig. 5C fits well with the theoretical red line.

To explain the enhancement in membrane binding of HS induced by LukF, the total concentrations of HS on the membranes ($[H_b]$) for applied $[H_o]$ in Fig. 2B2 were calculated from the association constants in Table 1. The calculated values (lines) gave a good fit to the experimental results (circles) for HS binding in the presence of LukF (Fig. 2B2).

2.2. Conclusion

- Various intermediate oligomers of γ-hemolysin was first time imaged at single-molecule level.
- 11 binding and association constants were estimated.
- The three cooperative stages (dimer-dimer interaction, single pore assembly, and aggregation of pores) substantially enhance the efficiency of assembly of oligomeric pores.
- We propose the model of assembly for γ-hemolysin in Fig. 6B.

In general, single-molecule observations and statistical analysis of populations of intermediates will be useful in understanding how single molecules are brought together into macromolecular complexes in cells.

3. Studying structural changes of LukF stem-domain during conversion from pre-pore to pore and Imaging pore-formation event

3.1. Results

3.1.1 Inactivation of cell lysis properties of double-cysteine mutants.

Three amino acid residues of LukF were selected for cysteine substitution,

including V12, which lies on the turn of the amino-terminal latch, and T117 and T136, located at the turns of the pre-stem domain, based on the Cβ-Cβ distances between pairs of amino acids (The Cβ-Cβ of V12–T136 ~ 0.9 nm, of T117-T136 ~ 0.5 nm, Fig. 7A and 7B). V12C-T136C, which had a single disulfide bond between the top of the cap and the pre-stem domain, was named Cap-Stem. The second mutant (T117C-T136C), Stem-Stem, had a disulfide bond between two β-strands of the pre-stem domain. Both mutants migrated faster than the wild type, because the internal disulfide bonds shortened the effective length of the SDS-denatured mutant proteins. The double-cysteine mutants are monomers having single-disulfide bonds

As shown in Fig. 8, both Cap-Stem and Stem-Stem in combination with Hlg2 exhibited no hemolysis. In contrast, once exposed to 20 mM βME, hemolytic activities of both mutants were restored to wild-type levels. The engineered disulfide bonds trapped the LukF pre-stem domain and prevented pore assembly, causing the loss of hemolysis.

3.1.2. Membrane binding ability of double-cysteine mutants

As shown in Figs. 3A and 3B, both double-cysteine mutants bound to HRBC membranes at about the same level as the wild type did whether or not their disulfide bonds were reduced by βME. This result demonstrates that trapping of the pre-stem domain by disulfide bond formation does not affect membrane binding of LukF.

3.1.3. Inhibition of the transition from pre-pores to pores by disulfide bond formation

We detected the SDS-stability of the oligomeric pre-pore formed by both double-cysteine mutants based on the intensities of the ~ 200kDa HMW bands (Fig. 9C). Similar patterns of HMW bands were obtained with LukF, Cap-Stem/(+)βME, Stem-Stem and Stem-Stem/(+)βME in lanes 4, 8, 10 and 12, respectively. The intensity of the HMW band from lane 10 of Stem-Stem was about 67% compared to that from lane 12 of Stem-Stem in the presence of βME. The two HMW bands in lanes 10 and 12 represented the pre-pore and pore, respectively, of Stem-Stem with Hlg2. By contrast, Cap-Stem failed to form an SDS-stable oligomeric complex with Hlg2. Nevertheless, exposure of both mutants to βME induced pore formation and cell lysis as indicated above and by HMW bands with intensities similar to that of wild-type LukF.

We then observed the structure of the pre-pore of Stem-Stem under a transmission electron microscope. The two images in Fig. 10B indicate that the SDS-stable pre-pores of Stem-Stem had ring-shaped structures similar to those of wild-type LukF.

3.1.4. Complete inhibition of oligomerization by low temperature

It was surprising to note that the hemolysis efficiency observed in Fig.11A with pore formation occurring at 2°C was almost equal to that at an incubation temperature of 37°C. The concentration for 50% hemolysis was about 8 nM in both cases. This result clearly proves that pore formation does not require high temperature, and indicates that

only the pre-pore oligomerization is a temperature-dependent stage. Therefore, we could effectively inhibit the pre-pore oligomerization by low temperature (2°C).

3.1.5. Slight inhibition of oligomerization by disulfide bond formation in Cap-Stem

We then investigated how formation of the disulfide bond locking the pre-stem back to the cap domain (Cap-Stem) affected the oligomerization of Cap-Stem. In fact, the hemolysis did occur after treatment of Cap-Stem as described above with βME at 2°C (Fig. 11B). The difference in hemolysis efficiency of Cap-Stem using these two conditions is indicative of the effect of disulfide bond formation on oligomerization through locking of the pre-stem domain to the cap domain. Although the hemolytic curve of pore formation performed at 2°C was shifted to a slightly higher concentration than that at 37°C, Cap-Stem was clearly still able to oligomerize with Hlg2 into pre-pores, which were then capable of transition to functional pores once the disulfide bond was reduced. These results show that disulfide bond formation in Cap-Stem inhibits pore formation, but only slightly inhibits pre-pore oligomerization.

3.1.6. Real-time observation of the transition of Stem-Stem from pre-pores to pores on a ghost cell.

It is necessary to test for pore formation using an ion size indicator to ascertain that no kind of pore is formed unless the disulfide bond is reduced. For a direct view, we imaged in real-time the transition from pre-pores to pores, as indicated by Ca^{+2} efflux through the pores. For visualizing the opening of pores, we detected Ca^{2+} release through pores formed on a Ca^{2+}loaded ghost cell, using a Ca^{2+} sensitive fluorescent dye (Rhod2 tripotassium salt cell impermeant) outside the cell. Before injection of βME (Fig. 12), image 0 s), the background was close to zero, indicating that no Ca^{2+} was released. Indeed, the pre-pores had not been converted to pores yet. At about 60 s after injecting βME into the chamber, many bright fluorescence spots progressively appeared with various intensities, as shown in sequential images of Fig. 6B from 60 s to 226 s. We designated those spots of Rhod2 signals as Ca^{2+} flames. Obviously, a Ca^{2+} flame appearance is associated with the transition from pre-pores to pores. And a Ca^{2+} flame reflects a cluster of pores. By 206 s, almost all the pores of the cell had opened, since after that new Ca^{2+} flames no longer appeared. The above evidence demonstrates the complete control of pore formation by disulfide bond formation in Stem-Stem.

3.2. Conclusion

Through the control of γ-hemolysin pore assembly using low temperature (2°C) and disulfide formation (S-S) in LukF mutants (Cap-Stem and Stem-Stem), we were able to

- Identify intermediate pre-pores and functional pores.

Propose the model of pore-formation for γ-hemolysin pore assembly, as follows:

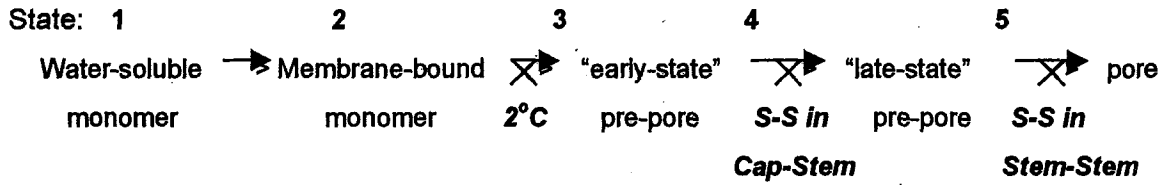

4. PUBLICATIONS

Nguyen, TV., Higuchi, H. and Kamio, Y. (2002) Controlling pore assembly of staphylococcal γ-hemolysin by low temperature and by disulfide bond formation in double-cysteine LukF mutants. *Mol. Microbiol.*, **45**, 1485-1498.

Nguyen, TV., Higuchi, H. and Kamio, Y. (2003) Single-molecule imaging of cooperative assembly of staphylococcal γ-hemolysin on erythrocyte membranes. *EMBO. J.*, 19, 4968-4979.

Monma N., Nguyen, TV., Yokota K., Higuchi, H. and Kamio, Y. (2003) Essential amino acids at LukF rim domain for Phosphatidylcholine-binding and pore-formation of staphylococcal γ-hemolysin on erythrocyte membranes. In preparation.

Data in figures	Constants		Concentrations of monomeric and oligomeric intermediates (μm^{-2})		
2A	K_F	2.1×10^{-4}			
	K_H	1.2×10^{-5}			
	R_F	2.0×10^{4}			
	R_H	1.8×10^{4}			
3B	K_{FH}	0.0010 ± 0.0003	$[F_1] = 3.8 \pm 0.6$	$[H_1] = 6.9 \pm 1.1$	$[F \cdot H] = 0.026 \pm 0.004$
3C	K_{F2+H}	0.081 ± 0.032	$[F_1] = 3.75 \pm 0.05$	$[F \cdot H] = 0.056 \pm 0.006$	$[F_2 \cdot H_1] = 0.017 \pm 0.003$
	K_{F+H2}	0.12 ± 0.084	$[H_1] = 0.27 \pm 0.02$	$[F \cdot H] = 0.056 \pm 0.006$	$[F_1 \cdot H_2] = 0.0017 \pm 0.0012$
	K_{F2+H2}	3.82 ± 1.23	$[F \cdot H] = 0.056 \pm 0.006$	$[F \cdot H] = 0.056 \pm 0.006$	$[F_2 \cdot H_2] = 0.012 \pm 0.003$
4	K_{F2+H2}	3.1 ± 1.1	$[F \cdot H] = 0.065 \pm 0.0092$	$[F \cdot H] = 0.065 \pm 0.0092$	$[F_2 \cdot H_2] = 0.013 \pm 0.0041$
	K_p	37 ± 14	$[F \cdot H] = 0.065 \pm 0.0092$	$[F_2 \cdot H_2] = 0.013 \pm 0.0041$	$[F_3 \cdot H_3] = 0.032 \pm 0.0063$
5A and B	K_{2p}	1.1 ± 0.22	$[F_3 \cdot H_3] = 0.24 \pm 0.019$	$[F_3 \cdot H_3] = 0.24 \pm 0.019$	$[F_6 \cdot H_6] = 0.066 \pm 0.010$
	K_{3p}	2.7 ± 0.68	$[F_3 \cdot H_3] = 0.24 \pm 0.019$	$[F_6 \cdot H_6] = 0.066 \pm 0.010$	$[F_9 \cdot H_9] = 0.043 \pm 0.0080$
	K_{4p}	3.4 ± 1.1	$[F_3 \cdot H_3] = 0.24 \pm 0.019$	$[F_9 \cdot H_9] = 0.043 \pm 0.0080$	$[F_{12} \cdot H_{12}] = 0.035 \pm 0.0075$
6A	K_{np}	3.0			

Table 1. Binding and association constants of intermediate stages in the pore assembly pathway. Binding and association constants are in units of μm^2; numbers of binding sites (R_F, R_H) are in μm^{-2}. Values are given as mean ± error, where error = mean x $n^{-0.5}$, and n is the number of measured spots. The values were calculated from the equations described in the Appendix.

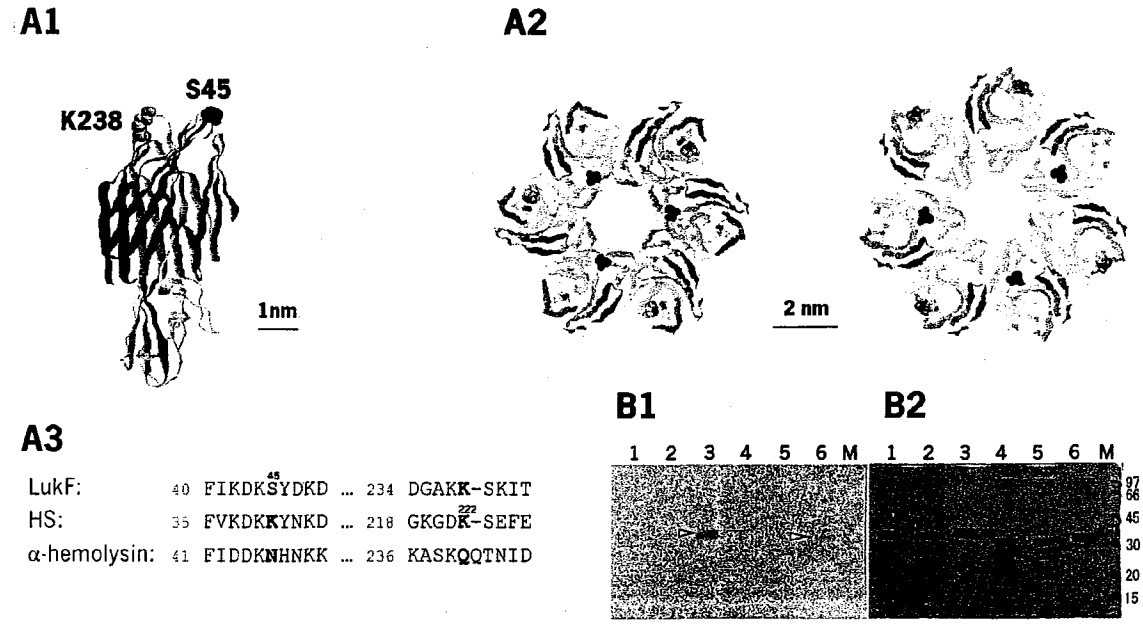

Fig. 1. Structures and labeling of LukF and HS

A. S45 (blue) of LukF and K222 (yellow) of HS (corresponding to K238 of LukF) were mutated to Cys, shown using the LukF structure (A1), the modelled g-hemolysin complex in hexamers or heptamers (A2), and the amino acid sequence alignment between LukF, HS, and a-hemolysin (A3). B. SDS-PAGE gels of 10 μg of fluorescently-labelled proteins, unstained (B1) and stained (B2) with Coomassie brilliant blue. Samples included LukF treated with TMR-maleimide (lane1), LukF-S45C (lane 2), LukF-TMR (lane 3, arrowhead), HS treated with IC5-maleimide (lane 4), HS-K222C (lane 5), and HS-IC5 (lane 6, arrowhead).

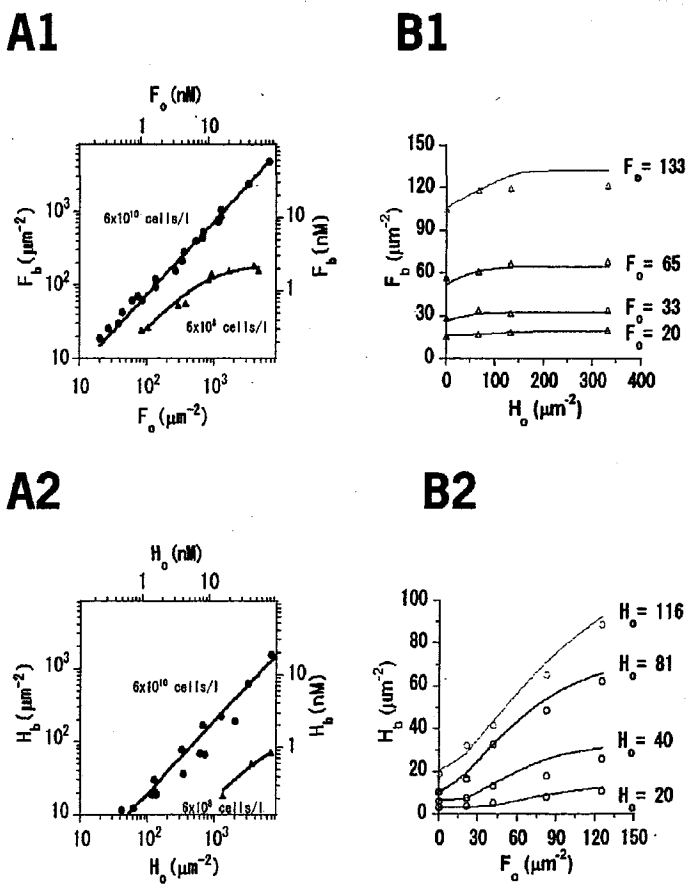

Fig. 2. Membrane binding of LukF and HS

A. Binding of LukF-TMR (A1) or HS-IC5 (A2). $[F_b]$ or $[H_b]$ were plotted against $[F_o]$ or $[H_o]$ at 6 x 10^{10} (●) and at 6 x 10^8 (▲) HRBC/l. The red lines represent the fitting of data (Appendix 1). B. Binding of both LukF-TMR and HS-IC5 to 6 x 10^{10} HRBC/l. At four values of $[F_o]$ (B1) and $[H_o]$ (B2), the relative $[F_b]$ and $[H_b]$ were measured in the presence of the other at different concentrations. The lines represent theoretical values of F_b (H_b), calculated based on the binding and association constants.

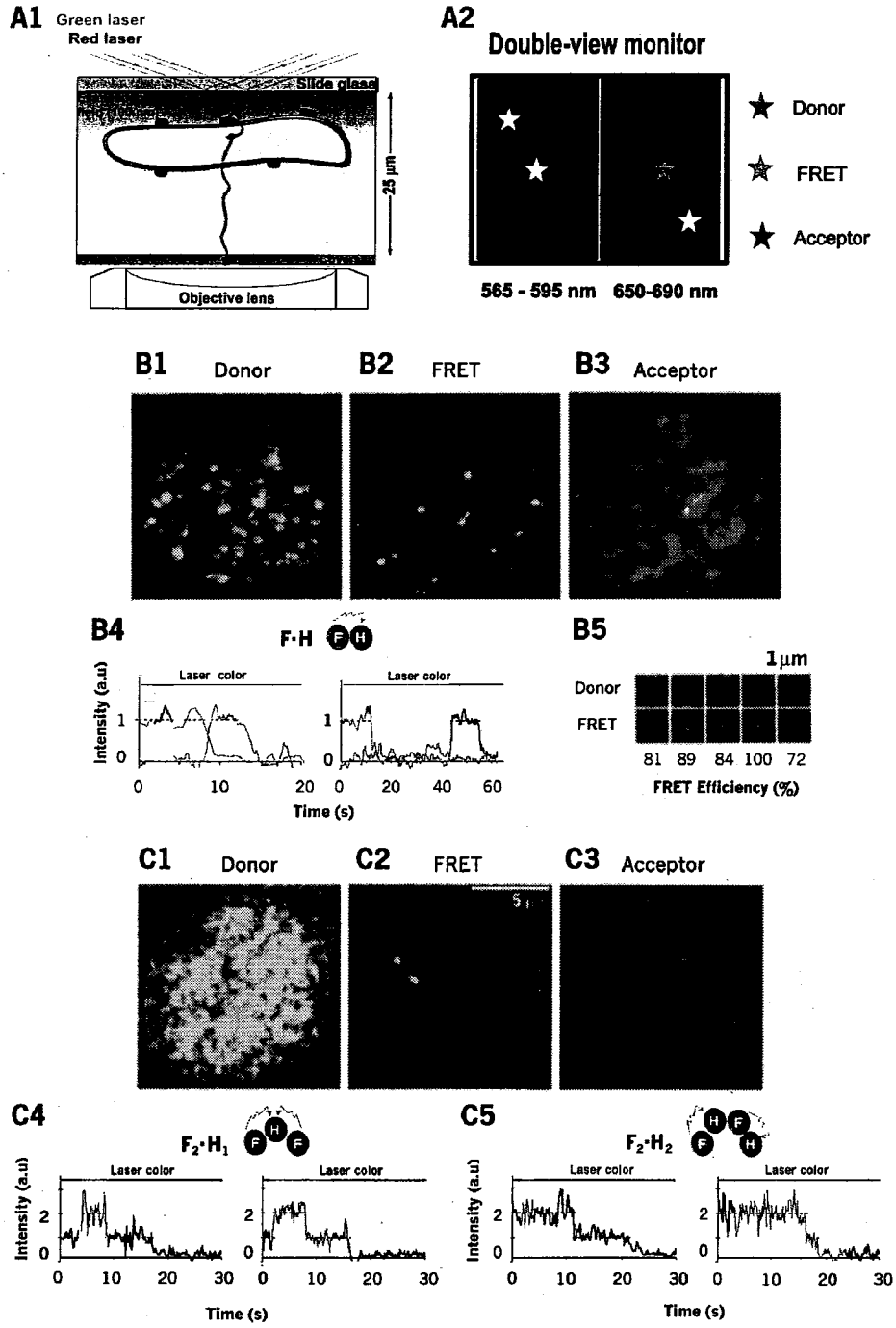

Fig. 3. Visualization of small oligomers of LukF and HS

A. Arrangement of the TIRF-microscope for observation of oligomerization on the membranes (A1). Fluorescence signals near the basal membrane appeared on the double-view monitor: the left is for the donor, the right is for FRET and the acceptor (A2). B and C. Images of dimers formed by LukF-TMR and HS-IC5 on HRBC membranes at low concentrations of proteins (75 pM and 750 pM, respectively) (B1-B3), and at higher concentrations of LukF-TMR (300pM) and lower HS-IC5 (200 pM) (C1-C3). TMR, FRET, and IC5 signals are shown after excitation by the green laser (B1 and B2; C1 and C2; time 0), and by the red laser (B3 and C3; time 0), respectively. B4 shows time traces of TMR (green), FRET (orange) and IC5 (red) emission corresponding to dimers (**F•H**=LukF-TMR·HS-IC5). The left (8 frame-averaged) indicates that IC5 photobleaches first, and the right (30 ms- interval) indicates that TMR photobleaches first. Five images of dual signals of TMR and FRET acquired from the same spots (B5). Thirty ms-interval time traces of acceptor emission on anticorrelated excitation by the green and red lasers for short (~ 3s) or long times (> 10 s) showing trimers ($\mathbf{F_2{\bullet}H_1}$, C4) and tetramers ($\mathbf{(F{\bullet}H)_2}$, C5).

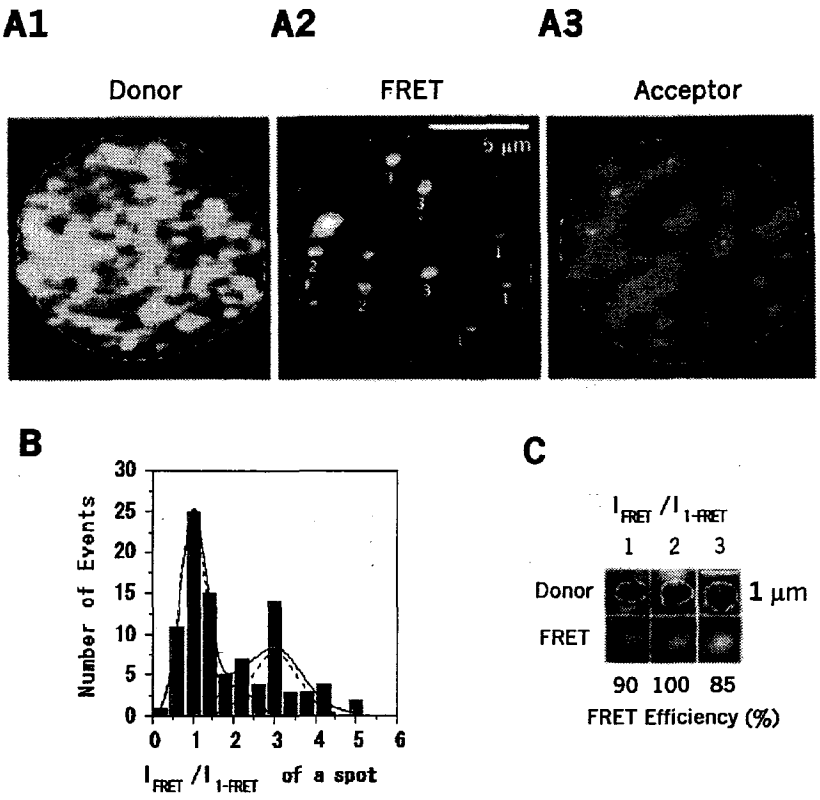

Fig. 4. Visualization of intermediate oligomers and single pores

LukF-TMR and HS-IC5 were incubated with HRBC at intermediate concentrations of 400 pM and 4 nM, respectively. White numbers on A2 indicate **m** in $F_m \cdot H_n$. B. Population histogram of intermediate oligomers: the dotted and solid lines indicate Gaussian distribution peaks for **F•H**, $(F \cdot H)_2$, $F_3 \cdot H_{3\text{-}4}$, and for the total population, respectively. C. Three images of dual signals of TMR and FRET-IC5, showing single and multi-molecule FRET efficiencies between LukF-TMR and HS-IC5 in oligomers.

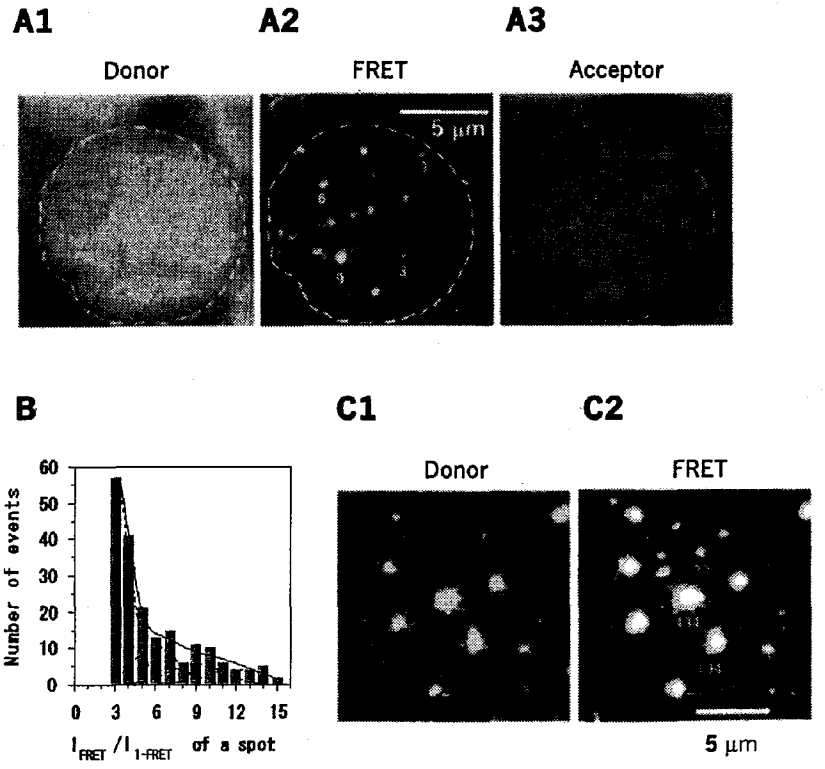

Fig. 5. Visualization of clusters of pores

LukF-TMR and HS-IC5 were incubated with HRBC at 1.5 nM and 15 nM (A), or of 15 nM and 150 nM (C), respectively. White numbers on A2 indicate **m** in $F_m \cdot H_n$. Blue numbers on C2 indicate the number of pores in each large spot. B. Histogram of populations of $F_m \cdot H_n$ corresponding to single pores and groups of pores at 15% hemolysis. The dotted and solid lines indicate Gaussian distribution peaks at single, two, three and four pores, and the total population, respectively.

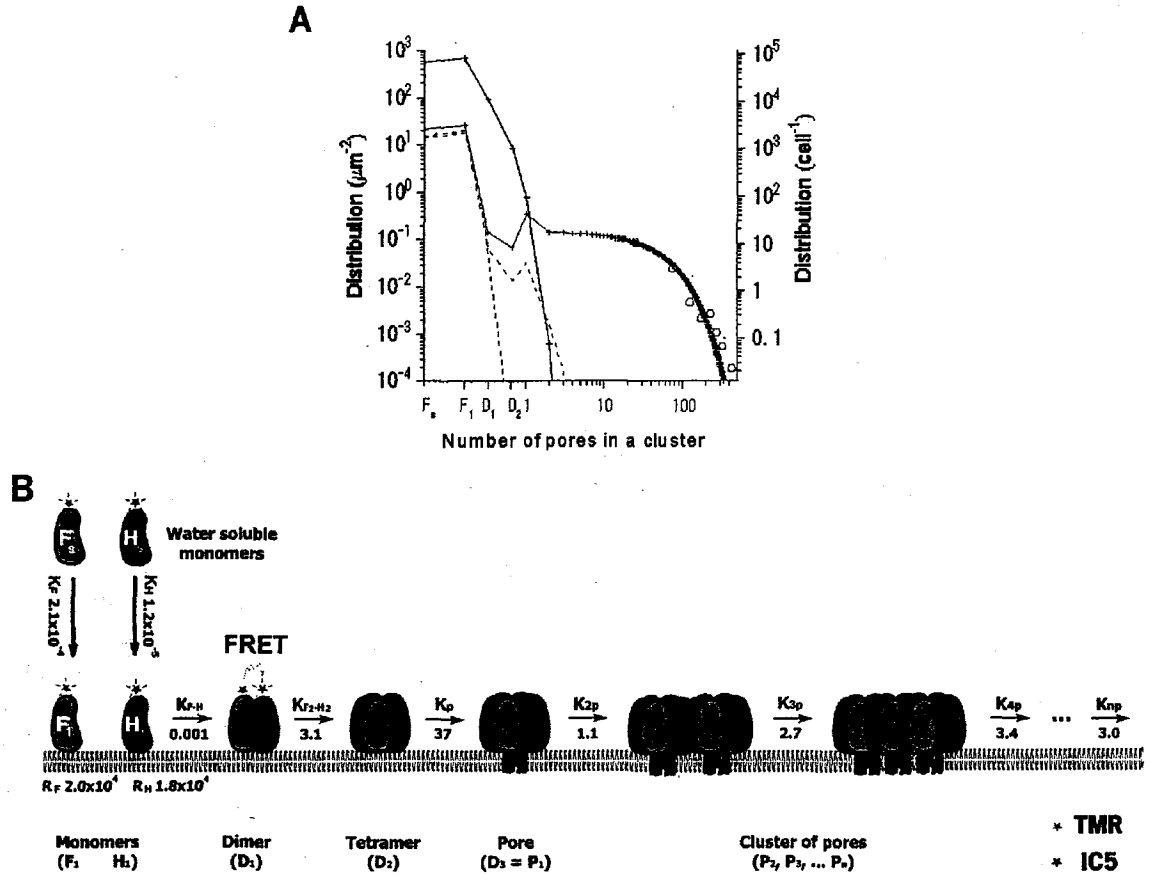

Fig. 6. Simulations and models for pore assembly

A. Experimental and theoretical distribution of intermediates at given protein concentrations (K_{np} is assumed ~ K_{3p} or K_{4p}). The blue circles were measured from 237 spots of data like Fig. 5C, and were fitted by the theoretical red line. The dotted and solid lines represent theoretical distributions at $[F_o]$ and $[H_o]$ of 25 and 1000 mm-2, respectively. The red lines represent a fully cooperative process, similar to natural conditions. The black lines represent non-cooperative processes (K of all stages are ~ $K_{F,H}$).

B. Cartoon model for pore assembly of LukF and HS. Water-soluble LukF (green) and HS (red) monomers bind to putative binding sites on the membranes. Sequentially, the membrane-bound monomers assemble into small oligomers (e.g. dimers and tetramers), then into single pores and clusters of pores. The pore is represented as a hexamer, although formation of hexameric and/or heptameric pores is possible. The FRET signals indicate oligomers. The blue lines indicate the transmembrane domains inserting through lipid bilayers upon pore formation. The numbers indicate equilibrium binding and association constants (μm2).

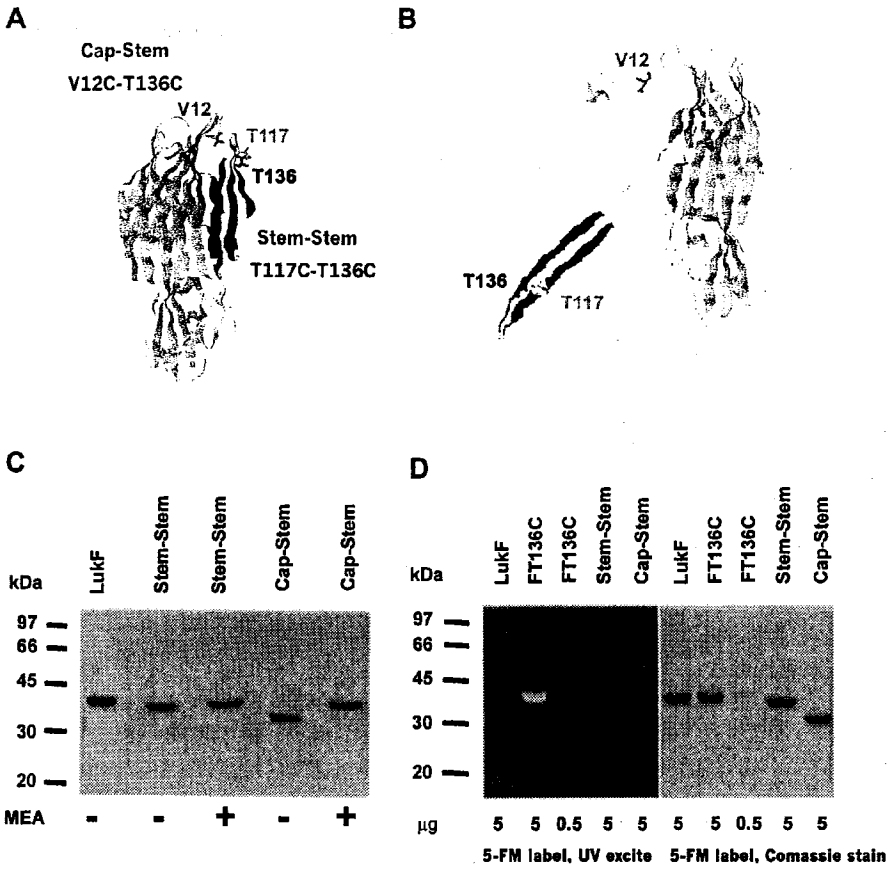

Fig. 7. Positions of amino acids for creating double-cysteine mutations in LukF

Ribbon representation of LukF monomer (A) and α-hemolysin protomer (B) featured with back-bond representation of amino acid residues mutated to cysteine: V12 (green), T117 (coban), T136 (red). The violet ribbon represents the pre-stem/stem domain. The two double-cysteine mutants generated were V12C-T136C (Cap-Stem) and T117C-T136C (Stem-Stem). (C) 5μg of purified proteins in all lanes in the presence and absence of βME were separated by SDS-PAGE, followed by staining with Coomassie brilliant blue. (D) SDS-PAGE gel of 5-FM labeled proteins using irradiation by UV-light (left) and Comassie staining (right) to detect the fluorescent label and all proteins, respectively.

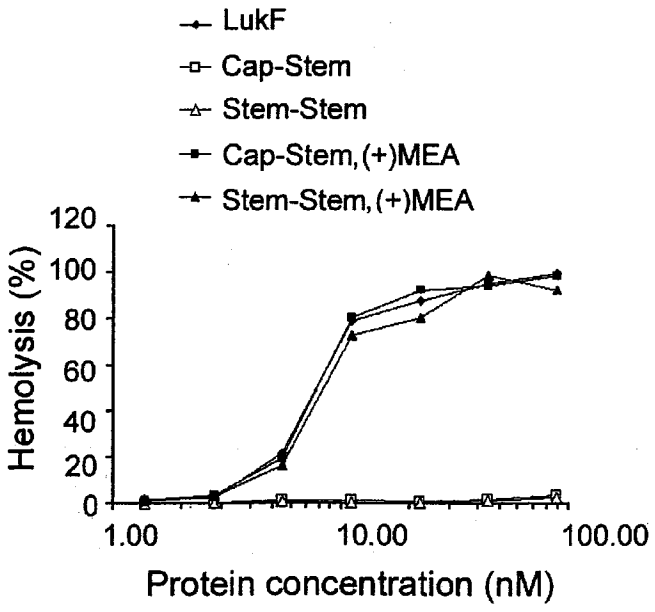

Fig. 8. Hemolytic activities of double-cysteine mutants induced by β-mercaptolethanol (βME).

Hemolytic activities of LukF or double-cysteine mutants in combination with Hlg2 at concentrations from about 2 to 100 nM toward 1% HBRC were analyzed at 37oC in the absence and presence of 20 mM βME

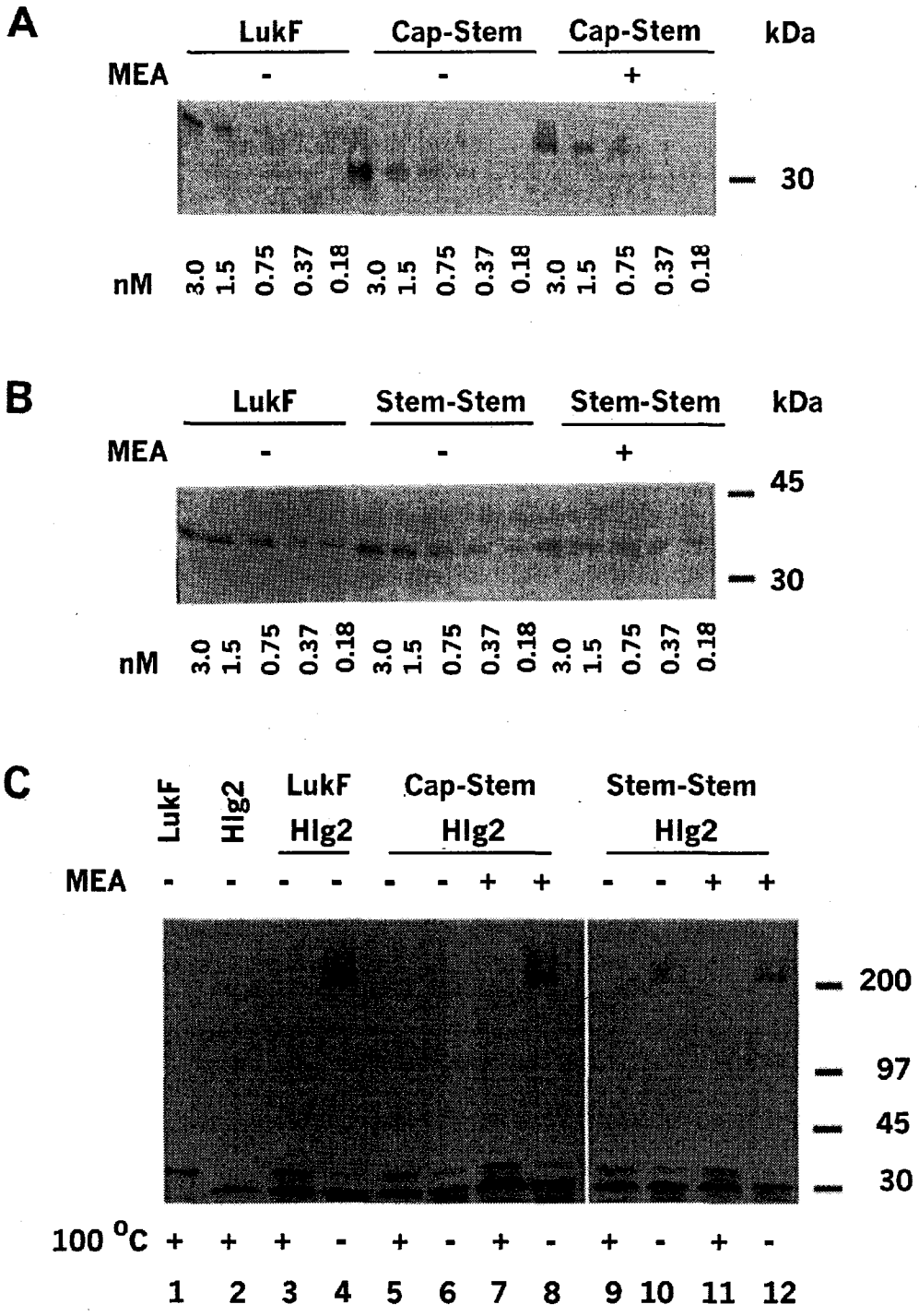

Fig. 9. SDS-PAGE detection of membrane binding, pre-pore oligomerization and pore formation of double-cysteine mutants

(A and B) Membrane binding: Proteins were applied into 1% HRBC at protein concentrations of 0.18 to 3.0 nM in the presence and absence of bME. Then, the membrane-bound monomer bands of LukF and Cap-Stem (A) and Stem-Stem (B) from solubilized membranes were separated by SDS-PAGE, visualized by Western blotting and immunostaining using antiserum against LukF. (C) Assembly into high-molecular weight complex: Proteins were applied into 1% HRBC at 30 nM, and the membranes were treated by 1% SDS at 20oC or 100oC, then were separated by SDS-PAGE with a linear gradient gel of 4-15% (w/v) acrylamide, and were analyzed by Western blotting and immunostaining using antisera against LukF and Hlg2. The intensities of complex bands were measured using NIH free software Scion 4.0.2.

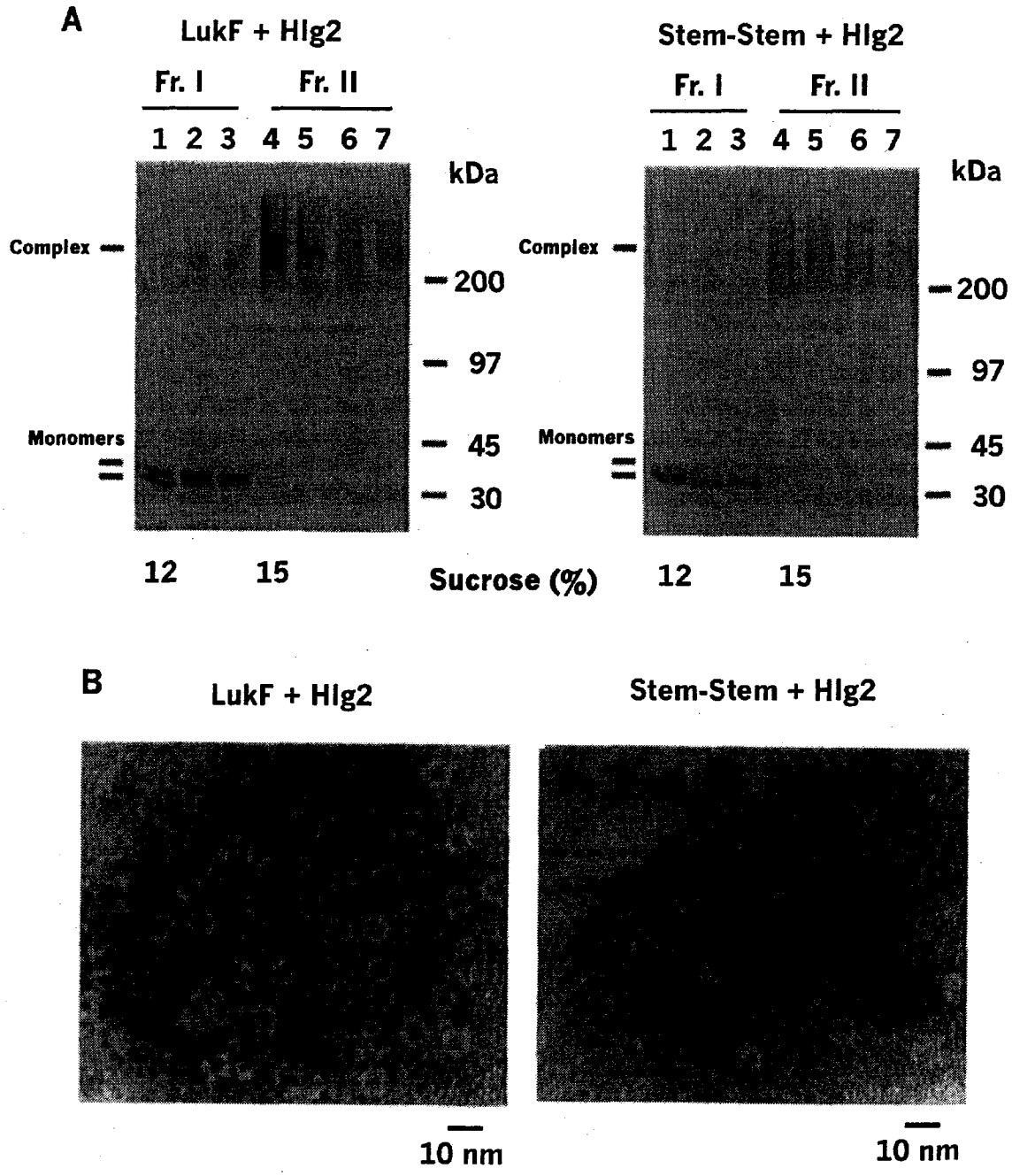

Fig. 10 Sucrose-gradient fractions and ring-shaped structures of isolated pores (LukF) and pre-pores (Stem-Stem)

Fractions 4-7 of LukF (A) and of Stem-Stem (B) containing the high-molecular-weight complexes from the sucrose were selected based on Western blotting and immunostaining using antisera against LukF and Hlg2. The combined fractions were negatively stained with 1% phosphotungstate sodium pH 7.2 and observed by transmission electron microscopy. (C) Isolated pores of LukF and Hlg2. (D) Isolated pre-pore of the disulfide bond-containing Stem-Stem and Hlg2.

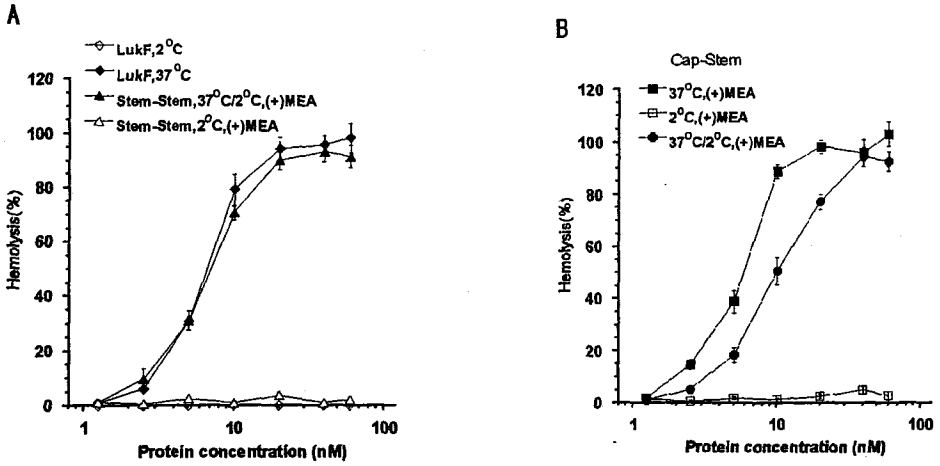

Fig. 11. Hemolytic activity of double-cysteine mutants induced by βME at low temperature

Hemolytic activity of LukF or double-cysteine mutants in combination with Hlg2 at about 2 to 100 nM against 1% HBRC was analysed under various incubation conditions. (A) LukF at 2°C and 37°C; Stem-Stem at 2°C with 20 mM βME; Stem-Stem at 37°C for 10 min, then 2°C for 30 min with 20 mM βME. (B) Cap-Stem at 2°C with 20 mM βME and 37°C with 20 mM βME; Cap-Stem at 37°C for 10 min, then 2°C for 30 min with 20 mM βME. Error bars represent the standard deviations of triplicate measurements.

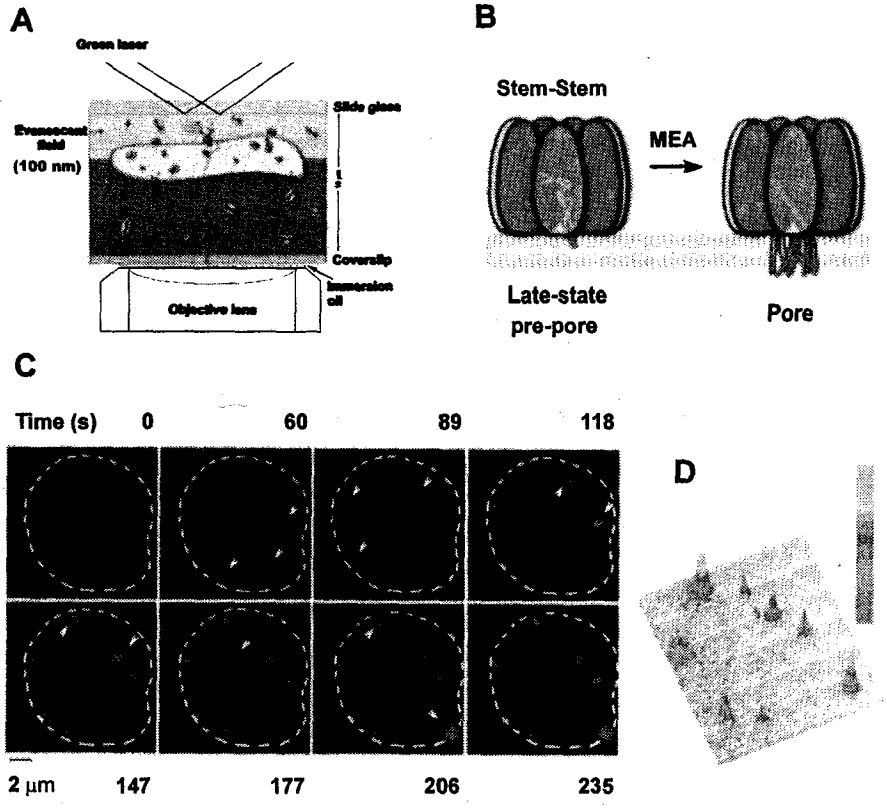

Fig. 12. Observation of the opening of pores formed by βME-treated Stem-Stem

(A) Ghost cells containing pre-pores of Stem-Stem (blue) were loaded with 10 mM Ca2+(yellow) inside, adhered onto the slide glass and put in a bath buffer containing 10 nM Rhod2 (gray), a Ca2+ sensitive fluorescence indicator. The pore opening was triggered by injection of 20 mM βME. Using TIRF-microscopy, signals of Rhod2 were monitored. The brightness of Rhod2 indicates the opening of one or clusters of pores. (B) 29 s interval sequential images showing consecutive pore-openings superimposed on a cell after 60 s of βME injection. (C) Distribution of Rhod2 signals on a cell in the 206 s image showing the density of Ca2+ efflux. Gradient of color from red to green represents gradient increase in intensity of the Rhod2 signal.

論文審査結果要旨

近年，黄色ブドウ球菌が人間を含む動物に重篤な疾患を引き起こすことが報告され，社会的に大きな問題となっている。その原因は，MRSA などの多剤耐性菌の出現，並びに細胞崩壊毒素による宿主細胞の崩壊にある。黄色ブドウ球菌は，感染に重要な白血球崩壊蛋白毒素ロイコシジン並びに赤血球崩壊蛋白毒素－ヘモリジンを大量に分泌する。主査の所属する研究室において，ロイコシジン及びγ－ヘモリジンの迅速高回収率単離精製法が確立されると共に両蛋白毒素遺伝子のクローン化に成功して，(1) 両毒素が LukF を共通成分とする 2 成分性膜孔形成毒素であること，(2) ロイコシジン遺伝子は新規溶原ファージφ PVL およびφ SLT ゲノム上に存在すること，(3) γ－ヘモリジンは LukF および Hlg2 がな 3 もしくは 3：4 比で交互に配置したヘテロ 7 量体の膜孔として作動すること，4) ロイコシジン活性には，LukF 及び LukS から成る膜孔形成に加えて LukS のリン酸化が必須であることなど膜孔形成毒素研究に新展開がもたらされた。さらに，LukF の標的細胞吸着，LukS 及び Hlg2 活性の標的細胞崩壊特異性に関わるアミノ酸残基膜膜孔形成過程の全容を解明した。本研究者の研究成果を要約すると，

(1) 標的細胞膜上における水可溶γヘモリジンステム領域の水不溶ステムへの劇的な構造変化を伴うステムの標的細胞膜貫通機構，『プレスム保有ヘテロ 7 量中間体』の発見，ならびにプレステムからステムへの移行タイミングの決定を行い，本成果を Molecular Microbiology に発表した。

(2) 膜孔葉合体で構成されるγ－ヘモリジンの「超チャネル」形成機構を「1 分子技法」を駆使して，以下に示す「超チャネル」形成までの全行程のリアルタイムでの句視化に成功した。そして膜上における『超チャネル』の形成機構は，① LukF の初発の膜への結合⇒② Hlg2 の LukF への結合⇒③［LukF-Hlg2］複合体形成⇒④［LukF-Hlg2］複合体 3 分子集合・6 量体形成⇒⑤ LukF もしくは Hlg2 の 6 量体への組込み・7 量体プレステム中間体形成⇒⑥ステムの伸長・膜孔形成⇒⑦膜孔集合・超チャネル形成，であることを証明した。

以上，本研究は広く生物由来の膜孔毒素の分子構築に新概念を植え付けたばかりでなく，細胞膜上における水可溶性蛋白質分子のダイナミックな構造変化を伴う不溶性膜孔『超チャネル』形成機構の理解に大きな示唆を与えた極めて国際的に評価の高い独創的な研究であると共に，毒素感染抑止剤の開発等，応用面においてもさらに進展する夢のある研究である。本成果は The EMBO Journal に発表された。

以上のことから審査員一同は，本研究者に博士（農学）の学位を授与するのに値するものと認定した。